Soft Matter

PAPER

Modeling and additive manufacturing of bio-inspired composites with tunable fracture mechanical properties

Cite this: *Soft Matter*, 2014, **10**, 4436

Leon S. Dimas and Markus J. Buehler*

Flaws, imperfections and cracks are ubiquitous in material systems and are commonly the catalysts of catastrophic material failure. As stresses and strains tend to concentrate around cracks and imperfections, structures tend to fail far before large regions of material have ever been subjected to significant loading. Therefore, a major challenge in material design is to engineer systems that perform on par with pristine structures despite the presence of imperfections. In this work we integrate knowledge of biological systems with computational modeling and state of the art additive manufacturing to synthesize advanced composites with tunable fracture mechanical properties. Supported by extensive mesoscale computer simulations, we demonstrate the design and manufacturing of composites that exhibit deformation mechanisms characteristic of pristine systems, featuring flaw-tolerant properties. We analyze the results by directly comparing strain fields for the synthesized composites, obtained through digital image correlation (DIC), and the computationally tested composites. Moreover, we plot Ashby diagrams for the range of simulated and experimental composites. Our findings show good agreement between simulation and experiment, confirming that the proposed mechanisms have a significant potential for vastly improving the fracture response of composite materials. We elucidate the role of stiffness ratio variations of composite constituents as an important feature in determining the composite properties. Moreover, our work validates the predictive ability of our models, presenting them as useful tools for guiding further material design. This work enables the tailored design and manufacturing of composites assembled from inferior building blocks, that obtain optimal combinations of stiffness and toughness.

Received 16th November 2013
Accepted 10th March 2014

DOI: 10.1039/c3sm52890a

www.rsc.org/softmatter

1. Introduction

Composites are an integral part of today's engineering world with applications in industries ranging from electrical to aerospace to automotive engineering. Due to their wide range of applications, considerable research effort has been devoted to elucidating the methods by which materials are combined to create optimal composites.[1–5] A significant portion of the work has focused on understanding the mechanisms by which composites can achieve great combinations of toughness and strength, as synthetic materials often fail in this regard.[6,7] In this effort, the study of biological systems has been especially fruitful. Experimental, computational and theoretical work has all been devoted to understanding and predicting the mechanisms of deformation and failure of natural composites.[8–15] These fundamental studies have decoded many of the basic mechanisms that form the basis of the superior mechanical performance of biocomposites.[16–20] In certain cases this decoding has also led to the realization of physical artifacts of bioinspired composites displaying mechanical properties similar to their biological predecessors.[21–25]

Biological composites typically have very distinct structural features at a wide range of length scales, spanning from just a few nanometers to the macroscopic scale.[8,12,15,20,26–30] Replicating these precise nanoscopic and mesoscopic geometries has been a particularly challenging aspect of the manufacturing of biomimetic composites. Several successful attempts have been made at creating composites with impressive fracture mechanical properties. However typically the manufacturing processes are either very expensive, time consuming or both and are not suited for industrial scale implementation.[22,31,32] Recently, additive manufacturing has showed the promise to be an effective technique to synthesize material systems at a range of length scales with complex topologies.[33–36] Some of the more recent advances in additive manufacturing technology include 3D printers capable of rapidly printing macroscopic composites with mesoscopic features consisting of materials with widely disparate mechanical properties. Although the resolution and the material selection of these machines can still be significantly improved, they already suggest the promise of creating advanced functional bioinspired composites.[23]

Laboratory for Atomistic and Molecular Mechanics (LAMM), Department of Civil and Environmental Engineering, Massachusetts Institute of Technology, 77 Massachusetts Ave., Cambridge, MA, USA. E-mail: mbuehler@MIT.EDU

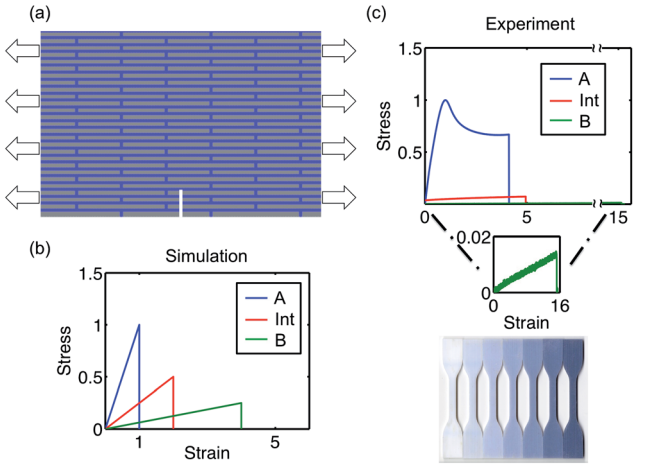

Fig. 1 (a) The model geometry with boundary conditions. (b) Three representative constitutive relations for the matrix phase of the composite in the computational work. In all systems the stiffest response represents the platelets. (c) Three constitutive relations for the matrix phase in the experimental study. Again, in all systems the stiffest response represents the platelet phase. Representative dogbone specimens forming the basis of the constitutive relations are also shown.

In this work we aim to investigate the efficacy of a natural design mechanism proposed in an earlier work.[37] Based on the computational investigation of a bone-like topology (Fig. 1) we proposed that we could fundamentally alter the deformation and fracture mechanism of the composite by tuning the interactions between the platelet and matrix phase. Moreover, we showed that by tuning these interactions in a conservative way we could create composites displaying both significant stiffness and fracture resistance. In this study we revisit these computational investigations and use them to qualitatively predict the response of 3D printed physical artifacts of the computationally conceived systems. We tune the interactions between the matrix and platelet phase in a bone-like topology and synthesize bioinspired composites that exhibit flaw insensitive deformation characteristics. Moreover, despite the limitations of the materials available for the 3D printing procedure (*i.e.* using inferior building blocks) we create composites that contain both stiffness and fracture resistance. Building on the work presented in ref. 23 we take a further step to validate our *de novo* approach to the design and synthesis of bioinspired composites. The study outlines the efficacy of 3D printing as a means of rapidly manufacturing complex functional composites designed and optimized through computer simulation.

2. Materials and methods

2.1 Experimental

The procedure of manufacturing, preparing and testing of the fracture specimens follows the procedure outlined in a previous study.[23] The specimens tested in this study are manufactured in the Precision Compliant Systems Lab (PCSL) at MIT on a Stratasys Connex500 multi-material 3D printer. We are able to manufacture composites with a variety of constituent materials in a single print. We use the two base materials VeroWhitePlus, a stiff proprietary acrylic monomer/oligomer mixture with a photoinitiator, and TangoBlackPlus, a soft proprietary urethane acrylate oligomer with a photoinitiator, with highly contrasting material properties (Fig. 1). These materials will henceforth be referred to as material A and material B respectively. The out-of-plane thickness of all manufactured specimens is 3.125 mm and the in-plane thickness of the soft phase in all composites is 250 μm. In all manufactured specimens the stiffer material A is used for the platelets in the bone-like topology (Fig. 1). We vary the constituent material for the matrix phase of the system and create nine different composites with an increasing stiffness ratio, ρ, where $\rho = E_p/E_m$. E_p and E_m represent the modulus of the platelets and matrix respectively. The materials cure almost immediately upon printing and the adhesion between different material phases is therefore close to perfect, *i.e.* the adhesion is as strong as the weakest phase. A representative selection of the constitutive behavior of the nine different materials used to represent the matrix is shown in Fig. 1. The stiffness ratio ρ varies over several orders of magnitude from unity, the bulk system consisting entirely of material A, to nearly one thousand, the matrix is composed entirely of material B. The seven systems with intermediate stiffness ratios are constructed by a mix of material A and B for the matrix phase. The mixing ratios are preprogrammed in the printer and cannot be changed in the current setup.

The material properties of the individual constituent materials are found by tensile testing of dogbone specimens. A subset of the dogbone samples is shown in Fig. 1. A representative composite specimen used for the fracture testing is shown in Fig. 2. Both mechanical tests are performed in an Instron 5582 Universal Testing Machine with an Instron 100 kN static load cell. We apply displacement boundary conditions and load the samples at a rate of 0.5 mm s^{-1} and 0.1 mm s^{-1} for the fracture specimens and dogbone specimens, respectively. The applied strain rate is bounded from above by our desire to approach static loading conditions and from below by practicality considerations. The compliant samples are very extensible and we wanted to ensure that the testing would finish in a reasonable amount of time. In both cases, the samples were clamped in place with serrated hardened steel grip faces attached to steel vice action grips. The load capacity of the grips is 100 kN and the spring stiffness of the entire testing device far exceeds the stiffness of our specimens. As shown in Fig. 2 aluminum strips were attached to the fracture specimens for optimal gripping. The aluminum strips were attached with Loctite E-90FL epoxy. This was not necessary for the dogbone samples as they are much smaller and thus transmit a significantly smaller force.

As in our earlier study the fracture specimens are notched with a 1/32″ thick carbide slitting slaw with a 60° included angle and all cracks originate from the crack tip. Both the dogbone specimens and the fracture specimens are loaded until complete failure with their complete force extension behavior recorded. It is clear that the experimental procedure here does not emulate ASTM, as this was never a motivation driving the experimental design. Our goal was to design an experimental approach that is close to our computational approach and that is suited for investigating deformation and fracture

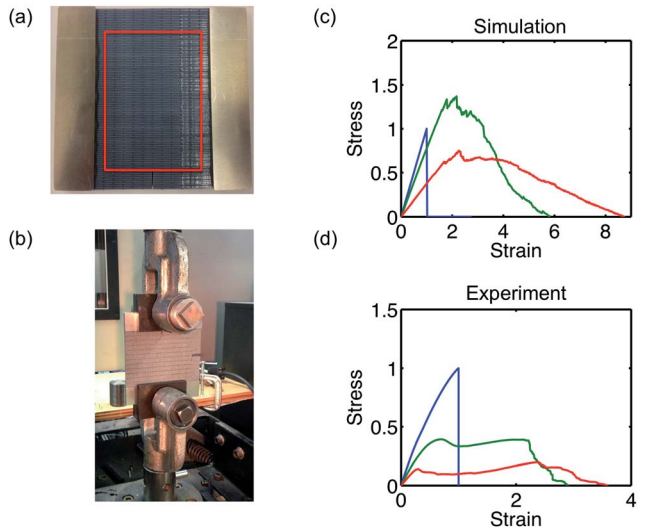

Fig. 2 (a) The sample geometry with aluminum strips glued on either side. The red box indicates the area on which DIC was performed. (b) Schematic of the experimental design. (c) Three representative stress *vs.* strain responses for the computational composites. The diagram indicates the large range of composite behavior obtained through tuning the interactions between the constituent phases. The response ranges from a stiff brittle behavior through a stiff, strong and tough behavior to a compliant and tough behavior. (d) Three representative stress *vs.* strain responses for the manufactured composites. Again, the diagram indicates the large range of composite behaviors obtained. However, due to the relative strength of material A the composites do not obtain superior strength. Nonetheless, they do outperform the bulk materials in terms of toughness modulus, see also Fig. 5.

mechanisms. The approach described and used here serves this purpose. We present this data in normalized stress–strain diagrams. The stresses are normalized by the peak stress of material A and the strains are normalized by the corresponding value of strain. We do this to simplify the comparison with our computational investigations. As the point of interest in this study is the comparison, absolute values of mechanical properties are of no particular interest.

We analyze strain fields in order to investigate the dominating deformation mechanisms in the composites. These prove helpful in understanding the mechanisms by which the topology of the specimen and the material properties of its constituents affect the composites mechanical performance. The experimental strain fields are obtained through digital image correlation (DIC). Speckle patterns are spray-painted on all samples with a range of grey tones to assist the DIC and we use the commercial software VIC-2D correlated solutions to analyze the images.

2.2 Computational

The computational results presented in this paper are based on the investigations presented in our previous work.[37,38] We study a mesoscopic system consisting of a compliant and stiffer phase arranged in a 'bone-like' topology (Fig. 1). The system is modeled as an assembly of springs and beads. The beads represent a coarse-graining of matter and the springs represent the bonds between particles. This type of model has been extensively used in independent research efforts and has been shown to be appropriate for mesoscopic systems.[39–41] The bulk constitutive relations for the two phases of the studied computational composite are given in Fig. 1, presented side by side with the constitutive relations of the experimental materials. We make no attempt at precisely replicating the experimental materials in our computational model. There are several reasons for this. Most importantly is the observed scatter in the experimental results. This high degree of variability surely does not warrant a precise parameterization of the computational springs. A more sophisticated modeling technique involving uncertainty propagation would be required to justify this. Furthermore, as was also discussed in ref. 37 there is likely a mixing of the constituent materials at the interfaces which can have a dramatic effect on the effective stiffness ratios. A simple calculation using Voigt's rule of mixtures showed that with a mere 3–4% mixing in the composite with the largest stiffness mismatch the stiffness ratio could shift by orders of magnitude. Accurately characterizing and modeling this interfacial mixing could become complex and does not seem sensible in the scope of this study. Indeed, it is the mechanisms we are most interested in and simple computational models are regarded to be of a significant value. Correspondingly we cannot expect our model to give accurate quantitative predictions for the response of the experimental system. Rather, we expect our model to capture the deformation and fracture mechanisms exhibited in the manufactured specimens. Therefore, as detailed in ref. 37 our model is designed to do exactly that.

2.3 Measured quantities to extract mechanical properties

Four measured quantities form the basis of the analysis presented in the following sections; the strain, the stress σ, the Young's modulus E and the toughness modulus T. We distinguish between a local strain ε_{ij} and a macroscopic tensile strain ε. The local strain tensor is calculated by means of the Zimmerman virial deformation measure[42] and this forms the basis for the strain fields presented in the computational investigations. The macroscopic tensile strain is calculated as an engineering strain by considering the change in length of the specimen. We use the virial stress as the stress measure[43] and the Young's modulus is calculated as the ratio of the uniaxial tensile stress to the uniaxial tensile strain.

Finally we characterize fracture resistance through the toughness modulus. The toughness modulus is defined as the area under the stress strain curve and can be interpreted as a metric of the required energy to fracture a system. The toughness modulus is a convenient measure of fracture resistance and it is a quantity typically used to describe the fracture resistance of biomaterials.[44]

3. Results

3.1 Stress *vs.* strain response

In Fig. 2 we display the stress strain response of both the computationally (Fig. 2b) and experimentally (Fig. 2c) tested

specimens. The stress strain curves represent the response of notched specimens. Both diagrams indicate a wide variation of composite behavior as the constitutive behavior of the matrix is tuned. The composites transition in behavior from very stiff and brittle to a complaint ductile response. For the composites with matrices of intermediate modulus ratios ρ, the stress *vs.* strain curves are indicative of a more robust mechanical response, with considerable stiffness and toughness modulus.

For the computationally tested specimens the stress strain response clearly indicates a superior mechanical performance for those composites with an intermediate stiffness ratio. This is not the case for the experimentally tested specimens. There are two plausible explanations for this which are motivated by Fig. 1. The constitutive relation for the platelets (material A), which is modeled as linearly elastic and perfectly brittle, is neither linearly elastic nor perfectly brittle. Rather, a considerable plastic regime can be identified in the stress strain curve. Correspondingly the stiff phase in the experimental setup is not as 'inferior' as in the computational investigation. Rather, the material B is the inferior constituent. In the computational investigation the constitutive relations of the matrix phase are parameterized to have the same toughness modulus as the platelet phase. In the original work this was argued to be a conservative estimate in the context of biomaterials.[37] However, as is also observed in Fig. 1, this is not the case for the acrylic materials used in this additive manufacturing process. The increased extensibility of the more compliant material B does not correspond to the massively inferior stiffness. The performance of the composites is constrained by the limited selection of materials available for printing. Nonetheless, it is instructive to analyze the deformation and fracture mechanisms of the respective experimental and computational composites. The fundamental nature of the design mechanism explored here is cemented by the observation that the proposed mechanisms persist in experiment.

To keep the following discussion concise and to the point we will be presenting data for three manufactured and computational specimens respectively; the bulk specimen, the composite with the most extreme stiffness ratio and a composite with an intermediate stiffness ratio. The stiffness ratio of the experimental intermediate stiffness ratio specimen is ~100 and ~4 for the corresponding computational specimen.

3.2 Deformation and fracture mechanisms

We start by comparing and analyzing the deformation mechanisms as encapsulated by the strain fields plotted in Fig. 3. Fig. 2a indicates the portion of the samples analyzed by DIC. The region of analysis was obtained by balancing the requirement of a high resolution for optimal correlation and that of a large area for a more complete comparison. The region behind the crack tip was omitted from analysis as discontinuities tend to disrupt the process of DIC. Fig. 3 shows three representative strain fields from both the computational as well as the experimental investigation. In both cases we display the strain field for the homogeneous specimen, a specimen with an intermediate stiffness ratio and that with the largest stiffness ratio. The images clearly suggest that the deformation mechanisms active

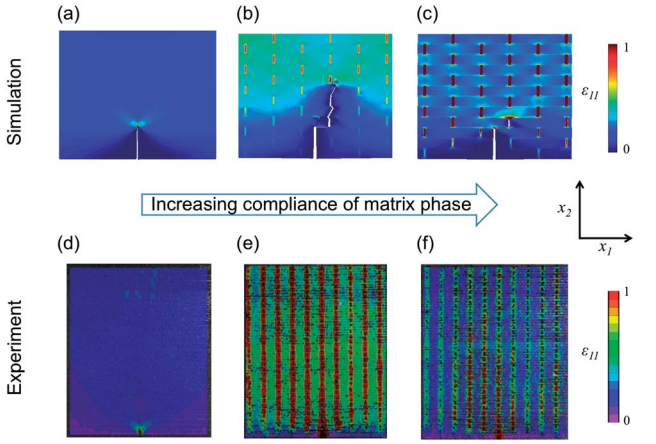

Fig. 3 (a–c) Strain fields for the three representative composites as predicted by simulation. Panel (a) displays the bulk system, the stiffness ratio is unity, panel (b) displays an intermediate stiffness ratio system and panel (c) displays the simulated composite with the largest stiffness ratio. (d–f) Strain fields as obtained by DIC for three representative synthesized composites. Similarly as for the simulated specimens, panel (d) displays the bulk system, panel (e) displays an intermediate stiffness ratio system and panel (f) displays the synthesized composite with the largest stiffness ratio. All strain fields for the simulated composites are plotted with the same color code and all experimentally tested composites are plotted with the same color code, see legend. Amongst themselves the strain fields from simulation and experiment are thus respectively quantitatively comparable. Comparisons between strain fields from simulation and experiment can only be made qualitatively. In both the computational and synthesized systems the increasing stiffness ratio leads to a delocalization of strains from the crack tip and a localization of strains in the distributed softer matrix phase. The inclusion of the softer matrix alleviates the loading on the crack tip; the crack tip is no longer the only critical flaw. Moreover, for both the simulated and synthesized systems in the intermediate stiffness ratio composite, the interactions between the constituent phases are fine tuned in a matter that allows a closer to uniform distribution of strain throughout the composite. The composites approach a flaw tolerant behavior and exhibit both significant stiffness and fracture resistance.

in the computational system and the experimental system are very similar. In both cases, the homogeneous system exhibits a characteristic strain concentration around the crack tip and relatively low strains in regions far from the crack tip. Considering the other extreme, an almost opposite deformation mechanism is observed. Rather than a single strain concentration around the crack tip, strain is concentrated around the distributed vertical portions of the soft matrix (non-optimal resolution in the experimentally obtained DIC images shows these local regions of high strain as continuous lines of higher strain). As predicted in earlier studies and by the computational work presented here, the low stiffness regions further from the crack tip serve as additional weak areas apt for strain localization. This distributed localization translates to delocalized deformation enabled by a 'distribution-of-weakness' mechanism active in the composites.

In the case of the composite with an intermediate stiffness ratio the agreement between the computational and experimental study is also quite remarkable. The stiffness ratio in the two systems is not the same and it is clear that the exact

distribution of strain is not identical in the two cases. Nevertheless, the mechanism is the same. Again, the 'distribution-of-weakness' effect leads to high tensile strains in the vertical portions of the soft phase. However, the intermediate stiffness ratio case distinguishes itself from the more extreme composite in that the stiff platelets also carry a significant portion of strain. The constituents of this composite exhibit a cooperativity far exceeding that observed in the other composites. As predicted by our computational investigation, it indeed seems possible to fine-tune the interactions between the individual constituents to achieve a near uniform distribution of strain in a cracked specimen. This mechanism has been proposed earlier,[17,37,45,46] but to the best of the authors' knowledge it has never before been demonstrated in a synthetic composite.

Fig. 4 shows snapshots of the fracture path in the two synthesized composites analyzed in Fig. 3 with $\rho > 1$. Fig. 4(a, c and e) shows that our computational studies correctly predict the intermediate stiffness ratio systems to exhibit initial evidence of crack arrest upon which further deformation causes critical crack propagation.[37] As the strain in the stiffer phase is so large in this composite, the crack naturally also propagates through the platelets. Correspondingly the crack propagation exhibits a more brittle nature. However, prior to catastrophic failure the composite does dissipate considerable energy through the mechanism of initial crack arrest (see also Fig. 2). In Fig. 4(b, d and f) we present the crack propagation in the synthesized composite with largest stiffness ratio. It is clear that the increased compliance of the matrix phase has fundamentally shifted the nature of the crack propagation. Rather than propagating through the platelets, the crack now travels almost exclusively through the soft matrix and the response of the composite has transitioned to a ductile one. It is noted that the results presented here for the large stiffness ratio sample are very similar to those presented in a previous study.[23]

The observations noted in the previous section highlight the significance of the accurately predicted deformation and fracture mechanisms. The consistency of these mechanisms between simulation and experiment, despite the disparate constitutive relations of the constituent phases, underlines the generality of the design mechanisms employed to construct these composites.

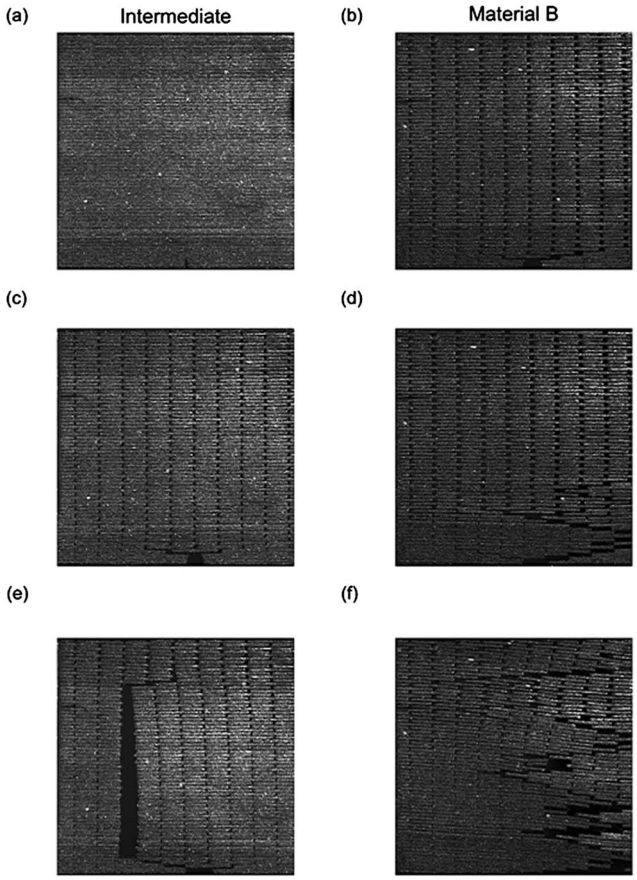

Fig. 4 Experimental results of fracture mechanisms for different stiffness ratios. (a, c and e) Snapshots displaying fracture propagation in a composite with intermediate stiffness ratio. Upon initial crack arrest the fracture propagates catastrophically through the platelets. (b, d, and f) Snapshots displaying fracture propagation in the composite with the largest stiffness ratio. Due to the extreme compliance and extensibility of the matrix phase the fracture travels almost exclusively through the softer phase. The presented images clearly indicate how the fracture path is strongly influenced by the stiffness ratio between the platelet and matrix phase.

3.3 Ashby plot analysis

Finally, an Ashby plot showing the relationship between toughness modulus and stiffness for both the computationally and experimentally tested composites is depicted in Fig. 5. First, we note that the results presented for the experimentally tested specimens here are not in agreement with the data presented in an earlier study.[23] The reason for this is that the materials used in this study are not the same as those used earlier. Since the last experiments the manufacturers have changed the chemistry of material A making it significantly stronger. Evidently, the same is not the case for material B. Nonetheless, the displayed Ashby plots exhibit similar trends. First, they show that both the computationally and experimentally tested composites span a large and advantageous portion of the Ashby area. This observation supports the hypothesis driving the study; that it is indeed possible to create a wide range of composites (and high performing composites) by simply tuning the constitutive relations of a matrix phase. Considering the typical performance of engineered composites this is an encouraging observation. The diagrams quite clearly portray that tuning the interactions of the composite constituent phases through controlling the stiffness ratio does fundamentally alter the fracture mechanical properties of the composite. Moreover, despite the superiority of material A, tailoring the composite interactions through the introduction of an inferior, more compliant matrix phase is capable of creating superior composites. Intuitively this might be a quite surprising finding; the introduction of a weaker material leads to a stronger composite. However, considering Fig. 3 and 4 it is quite clear that this is the case. The weaker phase shifts the nature of load transfer in the composite to a more advantageous one. Our simulations correctly predict that it is indeed an intermediate stiffness ratio that produces composites with optimal mechanical performance.

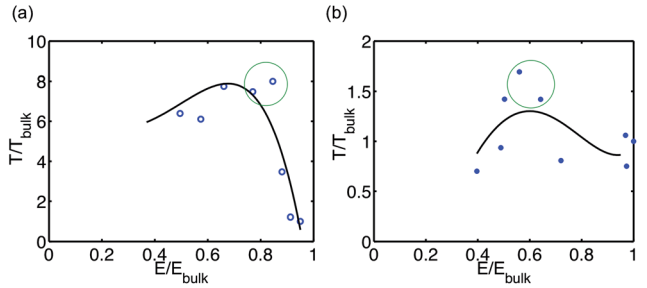

Fig. 5 (a) Ashby plot indicating the correlation between toughness modulus T and Young's modulus E for simulated composites. (b) Ashby plot indicating the correlation between toughness modulus T and Young's modulus E for experimentally tested composites. In agreement with the response predicted by our simulations the design mechanism succeeds to create synthetic composites with significant stiffness and superior fracture resistance, as measured by the toughness modulus. Moreover, in agreement with simulation the top performers of the synthesized composites are those with an intermediate stiffness ratio. For the particular constituent materials used here they in fact display a significantly greater toughness modulus than the most compliant composites. The optimal performers in both cases are circled. The fitted curves are fifth-degree polynomials fitted by minimizing the sum of residual square error and a non-zero regularization term.

4. Conclusions

Guided by computational investigations we have synthesized bioinspired composites that exhibit fracture mechanical characteristics superior to their constituents. By studying natural systems we abstracted key properties of biomaterials contributing to their impressive mechanical performance. Through computer simulations we elucidated key design mechanisms and based on these design mechanisms we synthesized composites with microfeatures through additive manufacturing. Specifically we predicted that given an appropriate topological arrangement, the interaction between a stiff and soft phase in a composite could be tuned to create material systems that would exhibit significant stiffness combined with superior toughness. Moreover, we predicted the interactions could be tailored to manufacture composites with superior flaw tolerance. Despite limitations in the range of materials available for printing, our experimental investigations confirmed our computational predictions. Importantly, we manufactured macroscale composites modeled after microscopic features of biological systems that exhibited deformation and fracture mechanisms akin to biomaterials. Future work could focus on improving the quantitative predictive power of our models.

Acknowledgements

Support was provided by ARO and ONR.

References

1 M. J. Biercuk, M. C. Llaguno, M. Radosavljevic, J. K. Hyun, A. T. Johnson and J. E. Fischer, *Appl. Phys. Lett.*, 2002, **80**, 2767.
2 J. N. Coleman, U. Khan, W. J. Blau and Y. K. Gun'ko, *Carbon*, 2006, **44**, 1624.
3 A. C. Balazs, T. Emrick and T. P. Russell, *Science*, 2006, **314**, 1107.
4 P. M. Ajayan and J. M. Tour, *Nature*, 2007, **447**, 1066.
5 S. Deville, E. Saiz, R. K. Nalla and A. P. Tomsia, *Science*, 2006, **311**, 515.
6 H. D. Espinosa, J. E. Rim, F. Barthelat and M. J. Buehler, *Prog. Mater. Sci.*, 2009, **54**, 1059.
7 M. F. Ashby, L. J. Gibson, U. Wegst and R. Olive, *Proc. R. Soc. A*, 1995, **450**, 123.
8 J. Aizenberg, J. C. Weaver, M. S. Thanawala, V. C. Sundar, D. E. Morse and P. Fratzl, *Science*, 2005, **309**, 275.
9 N. Almqvist, Y. Delamo, B. L. Smith, N. H. Thomson, Å. Bartholdson, R. Lal, M. Brzezinski and P. K. Hansma, *J. Electron Microsc.*, 2001, **202**, 518.
10 L. S. Dimas, G. H. Bratzel, I. Eylon and M. J. Buehler, *Adv. Funct. Mater.*, 2013, **23**, 4629.
11 P. Fratzl, H. S. Gupta, E. P. Paschalis and P. Roschger, *J. Mater. Chem.*, 2004, **14**, 2115.
12 P. Fratzl and R. Weinkamer, *Prog. Mater. Sci.*, 2007, **52**, 1263.
13 H. J. Gao, B. H. Ji, I. L. Jager, E. Arzt and P. Fratzl, *Proc. Natl. Acad. Sci. U. S. A.*, 2003, **100**, 5597.
14 C. E. Hamm, R. Merkel, O. Springer, P. Jurkojc, C. Maier, K. Prechtel and V. Smetacek, *Nature*, 2003, **421**, 841.
15 S. Weiner and H. D. Wagner, *Annu. Rev. Mater. Sci.*, 1998, **28**, 271.
16 S. Keten, Z. P. Xu, B. Ihle and M. J. Buehler, *Nat. Mater.*, 2010, **9**, 359.
17 K. Okumura and P. G. de Gennes, *Eur. Phys. J. E*, 2001, **4**, 121.
18 D. Sen and M. J. Buehler, *Sci. Rep.*, 2011, **1**, 35.
19 K. Tai, M. Dao, S. Suresh, A. Palazoglu and C. Ortiz, *Nat. Mater.*, 2007, **6**, 454.
20 S. Weiner, W. Traub and H. D. Wagner, *J. Struct. Biol.*, 1999, **126**, 241.
21 A. Finnemore, P. Cunha, T. Shean, S. Vignolini, S. Guldin, M. Oyen and U. Steiner, *Nat. Commun.*, 2012, **3**, 966.
22 Z. Y. Tang, N. A. Kotov, S. Magonov and B. Ozturk, *Nat. Mater.*, 2003, **2**, 413.
23 L. S. Dimas, G. H. Bratzel, I. Eylon and M. J. Buehler, *Adv. Funct. Mater.*, 2013, **23**, 4629.
24 S. M. Douglas, H. Dietz, T. Liedl, B. Hogberg, F. Graf and W. M. Shih, *Nature*, 2009, **459**, 414.
25 E. Dujardin and S. Mann, *Adv. Mater.*, 2002, **14**, 775.
26 F. Barthelat, *Bioinspiration Biomimetics*, 2010, **5**, 3.
27 F. Barthelat and H. D. Espinosa, *Exp. Mech.*, 2007, **47**, 311.
28 D. Losic, R. J. Pillar, T. Dilger, J. G. Mitchell and N. H. Voelcker, *J. Porous Mater.*, 2007, **14**, 61.
29 M. A. Meyers, P. Y. Chen, A. Y. M. Lin and Y. Seki, *Exp. Mech.*, 2008, **53**, 1.
30 J. Y. Rho, L. Kuhn-Spearing and P. Zioupos, *J. Biomed. Eng.*, 1998, **20**, 92.
31 G. D. Zhan, J. D. Kuntz, J. L. Wan and A. K. Mukherjee, *Nat. Mater.*, 2003, **2**, 38.
32 P. Podsiadlo, A. K. Kaushik, E. M. Arruda, A. M. Waas, B. S. Shim, J. D. Xu, H. Nandivada, B. G. Pumplin, J. Lahann, A. Ramamoorthy and N. A. Kotov, *Science*, 2007, **318**, 80.

33 D. Bak, *Assembly Automation*, 2003, **23**, 340.
34 D. Dimitrov, K. Schreve and N. de Beer, *Rapid Prototyping Journal*, 2006, **12**, 136.
35 E. A. Roth, T. Xu, M. Das, C. Gregory, J. J. Hickman and T. Boland, *Biomaterials*, 2004, **25**, 3707.
36 H. Seitz, W. Rieder, S. Irsen, B. Leukers and C. Tille, *J. Biomed. Mater. Res., Part B*, 2005, **74**, 782.
37 L. S. Dimas and M. J. Buehler, *J. Mater. Res.*, 2013, **28**, 1295.
38 L. S. Dimas and M. J. Buehler, *Bioinspiration Biomimetics*, 2012, **7**, 3.
39 W. A. Curtin and H. Scher, *J. Mater. Res.*, 1990, **5**, 535.
40 M. S. Daw and M. I. Baskes, *Phys. Rev. B: Condens. Matter Mater. Phys.*, 1984, **29**, 6443.
41 H. J. Gao and P. Klein, *J. Mech. Phys. Solids*, 1998, **46**, 187.
42 J. A. Zimmerman, D. J. Bammann and H. J. Gao, *Int. J. Solids Struct.*, 2009, **46**, 238.
43 D. H. Tsai, *J. Chem. Phys.*, 1979, **70**, 1375.
44 G. Mayer, *Science*, 2005, **310**, 1144.
45 B. H. Ji and H. J. Gao, *J. Mech. Phys. Solids*, 2004, **52**, 1963.
46 B. H. Ji and H. J. Gao, *Mater. Sci. Eng., A*, 2004, **366**, 96.